Available online at www.sciencedirect.com
ScienceDirect
International Journal of Heat and Fluid Flow 27 (2006) 887–894
International Journal of HEAT AND FLUID FLOW
www.elsevier.com/locate/ijhff

Parametric study of surfactant-induced drag-reduction by DNS

Bo Yu [a], Yasuo Kawaguchi [b,*]

[a] Department of Oil and Gas Storage and Transportation Engineering, China University of Petroleum, Beijing 102249, People's Republic of China
[b] Turbomachinery Research Group, National Institute of Advanced Industrial Science and Technology, 1-2 Namiki, Tsukuba, Ibaraki 305-8564, Japan

Received 26 August 2005; received in revised form 25 February 2006; accepted 4 March 2006
Available online 27 June 2006

Abstract

The effect of rheological parameters on the drag-reduction by surfactant additives is studied with a viscoelastic Giesekus model. It is found that the streamwise vorticity becomes much weaker and more elongated with the increase of large drag-reduction rates. The modifications of streamwise vorticity are given. The alteration of the energy cascade process is discussed.

Keywords: Surfactant; DNS; Drag-reduction; Giesekus model; Rheological parameters

1. Introduction

In a previous DNS study (Yu et al., 2004), a viscoelastic Giesekus model (Giesekus, 1982) was adopted to model the interaction between the network structures made up of rod-like micelles and solvent for the simulation of a 75 ppm surfactant solution at Reynolds number of around ten thousand. The numerical results qualitatively agreed with the experimental data, indicating that the Giesekus model is appropriate for surfactant solutions. Experiments showed that surfactant-induced drag-reduction is closely associated the concentration of the solution (Li et al., 1998). This is because the rheological properties vary greatly with the concentration (Kawaguchi et al., 2003). Therefore, it is interesting and necessary to perform a systematic investigation to study the effect of rheological properties on the turbulence structures and drag-reduction rate to further clarify the turbulent transport mechanism in drag-reducing flow. To develop a viscoelastic model for engineering applications, we need to establish a DNS database covering a wide range of rheological properties. For these scientific and engineering reasons, we carried out a series of runs for the surfactant solution with a faithful finite difference scheme (Yu and Kawaguchi, 2004) for a fully developed channel flow.

2. Numerical method

The drag-reduction by surfactant additives is related to the elasticity of the network structures formed by the rod-like micelles in the solution (Yu et al., 2004). We employed a viscoelastic Giesekus constitutive equation to model the interaction between the elastic network structures and solvent. The dimensionless governing equations for a fully developed turbulent channel flow can be written as

$$\frac{\partial u_i^+}{\partial x_i^*} = 0 \tag{1}$$

$$\frac{\partial u_i^+}{\partial t^*} + u_j^+ \frac{\partial u_i^+}{\partial x_j^*} = -\frac{\partial p^+}{\partial x_i^*} + \frac{\beta}{Re_\tau}\frac{\partial}{\partial x_j^*}\left(\frac{\partial u_i^+}{\partial x_j^*}\right) + \frac{1-\beta}{We_\tau}\frac{\partial c_{ij}^+}{\partial x_j^*} + \delta_{1i} \tag{2}$$

$$\frac{\partial c_{ij}^+}{\partial t^*} + \frac{\partial u_{\mathrm{m}}^+ c_{ij}^+}{\partial x_{\mathrm{m}}^*} - \frac{\partial u_i^+}{\partial x_{\mathrm{m}}^*} c_{mj}^+ - \frac{\partial u_j^+}{\partial x_{\mathrm{m}}^*} c_{mi}^+ + \frac{Re_\tau}{We_\tau}\left[c_{ij}^+ + \alpha(c_{im}^+ - \delta_{im})(c_{mj}^+ - \delta_{mj}) - \delta_{ij}\right] = 0 \tag{3}$$

where c_{ij}^+ is the conformation tensor associated with the deformation of the network structures. Re_τ ($Re_\tau = \rho U_\tau h/$

* Corresponding author. Fax: +81 29 861 7275.
E-mail address: yasuo@rs.noda.tus.ac.jp (Y. Kawaguchi).

0142-727X/$ - see front matter © 2006 Elsevier Inc. All rights reserved.
doi:10.1016/j.ijheatfluidflow.2006.03.013

Nomenclature

c	conformation tensor
C	mean conformation tensor
DR*%	drag-reduction rate (the reduction of friction factor with respect to Newtonian fluid at equal mean Reynolds number Re^*_m)
E	elastic energy $= \frac{1}{2}\frac{\eta}{\lambda} tr(c)$
f	friction factor $= 2\tau_w/\rho U_b^2$
h	half height of the channel
$\overline{k_e}$	mean elastic energy of the network structures over space and time
p	pressure
Re^*_m	Reynolds number $= 2\rho U_b h/\eta_w$
Re_τ	Reynolds number $= \rho U_\tau h/\eta_0$
Re^*_τ	Reynolds number $= \rho U_\tau h/\eta_w$
t	time
u	velocity
$\overline{u^+_{rms}}$	average root-mean-square of the streamwise velocity over space and time
$\overline{v^+_{rms}}$	average root-mean-square of the wall-normal velocity over space and time
$\overline{w^+_{rms}}$	average root-mean-square of the spanwise velocity over space and time
U	mean velocity
U_b	mean bulk velocity
U_τ	friction velocity $= \sqrt{\tau_w/\rho}$
$-\overline{u'^+ v''^+}$	Reynolds shear stress
We_τ	Weissenberg number $= \rho\lambda U_\tau^2/\eta_0$
x	spatial coordinate
y^*	dimensionless coordinate $= y/h$
y^+	$= y^* \times Re_\tau$
y^{+*}	$= y^* \times Re^*_\tau$

Greek symbols

α	mobility factor
β	ratio $= \frac{\eta_s}{\eta_0}$
δ^{+*}_{urms}	peak value position of the RMS of the streamwise velocity fluctuation base on the effective viscosity at the wall η_w
$\overline{v_t}$	the mean turbulent viscosity over space and time
ϖ	vorticity
η_a	dynamic shear viscosity of surfactant contribution
η_s	dynamic shear viscosity of solvent contribution
η_0	viscosity of the surfactant solution at zero-shear rate
η_w	the effective viscosity at the wall
λ	relaxation time

η_0) is the frictional Reynolds number based on the frictional velocity, half of the channel height and zero-shear rate viscosity. We_τ ($We_\tau = \rho\lambda U_\tau^2/\eta_0$) is Weissenberg number. Mobility factor α is a key parameter in determining the extensional viscosity. β is the ratio of solvent viscosity η_s over the zero-shear rate solution viscosity η_0 ($\eta_0 = \eta_a + \eta_s$, η_a is the contribution of surfactant additive).

The various rheological parameters shown in Table 1 are investigated to identify their effects on drag-reduction with a fixed Reynolds number, $Re_\tau = 150$. Dimitropoulos et al. (1998) studied the effect of the variation of rheological parameters with a Giesekus model. Their studies were for dilute solutions with β no more than 0.9 and the maximum drag-reduction rate was 44%. In order to get a larger drag-reduction rate, smaller β values are adopted in this study. The numerical method used here is a fractional-step method. The Adams–Bashforth scheme is used for time-advancement to ensure second-order accuracy in time. The second-order faithful finite difference scheme of Yu and Kawaguchi (2004) is used to enhance the numerical stability.

3. Results and discussion

The Reynolds number based on the effective viscosity, $\eta_w = \eta_0(\beta dU^+/dy^+ + (1-\beta)C^+_{xy}/We_\tau)/(dU^+/dy^+)$, at the wall is used for data reduction (Sureshkumar et al., 1997). The drag-reduction (DR) rate is defined as the reduction of the friction factor with respect to a Newtonian fluid at an equal mean Reynolds number, where the frictional factors of Newtonian fluid are evaluated by Dean's equation (Dean, 1978).

Some important results are listed in Tables 1 and 2. Table 1 shows that the DR rate increases with the increase of We_τ, with the decrease of α and with the decrease of β. Fig. 1 shows the velocity profiles. All the velocity profiles collapse in the viscous sublayer, and the velocity profile upshifts further in the bulk flow region with the increase of DR rate. Table 2 shows that generally speaking, larger DR rates are associated with larger $\overline{u^+_{rms}}$, smaller $\overline{v^+_{rms}}$ and

Table 1
Computational parameters and some important results

Fluid	β	We_τ	α	η_0/η_w	U^+_m	Re^*_τ	Re^*_m	DR*%
A	0.5	8	0.001	1.107	15.08	166	5000	0
B	0.5	12.5	0.001	1.184	18.14	178	6440	25.4
C	0.5	20.0	0.001	1.311	22.14	197	8710	46.0
D	0.5	30.0	0.001	1.455	25.92	218	11300	57.9
E	0.5	40.0	0.001	1.533	30.36	230	13970	67.7
F	0.5	50.0	0.001	1.598	33.32	240	15980	72.0
G	0.5	20.0	0.01	1.668	22.33	250	11180	43.5
H	0.3	30.0	0.001	1.907	29.15	286	16670	63.4
I	0.8	30.0	0.001	1.126	22.06	169	7450	46.3
N	–	–	–	1.000	14.78	150	4440	–

*Based on η_w. A–I denote viscoelastic fluids and N denotes Newtonian fluid.

Table 2
Some important results

DR^*%	Fluid	$\overline{u^+_{rms}}$	$\overline{v^+_{rms}}$	$\overline{w^+_{rms}}$	δ^{+*}_{urms}	δ^{+*}_{uu}	δ^{+*}_{vv}	$\overline{v_t}$	$\overline{k_e}$
0	A	1.46	0.570	0.721	11.2	130	26	9.1	0.40
25.4	B	1.65	0.528	0.679	17.1	166	42	8.6	0.62
43.5	G	1.85	0.526	0.684	20.3	234	58	8.4	0.47
46.0	C	1.98	0.474	0.634	22.2	215	46	8.4	0.98
46.3	I	2.18	0.479	0.679	22.2	211	52	8.1	0.65
57.9	D	2.48	0.433	0.588	28.6	307	68	6.5	1.39
63.4	H	2.68	0.402	0.564	32.3	358	89	5.0	2.02
67.7	E	2.75	0.349	0.515	30.2	323	72	4.1	1.79
72.0	F	3.19	0.308	0.474	36.3	486	75	3.2	2.01
–	N	1.43	0.593	0.747	12.2	94	35	10.9	–

The overbar means the average value over space (x, y and z) and time.

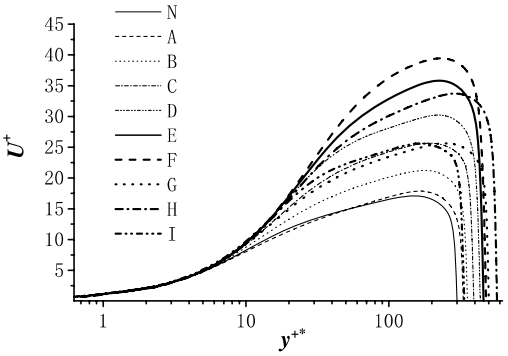

Fig. 1. Velocity profiles.

smaller $\overline{w^+_{rms}}$. With the increase of DR rate, the peak value position δ^{+*}_{urms} of the RMS of the streamwise velocity fluctuation shifts further to the bulk flow region. δ^{+*}_{uu} and δ^{+*}_{vv} are mean spacing between low-speed streaks and mean diameter of streamwise vortex at $y^{+*} = 15$, which are estimated by the separation of minimum spanwise two-point correlations R_{uu} and R_{vv}. Generally, large DR rates are related to large δ^{+*}_{uu} and δ^{+*}_{vv}. $\overline{v_t}$ and $\overline{k_e}$ are the mean turbulent viscosity of the flow and mean elastic energy of the network structures, respectively. The mean turbulent viscosities of all the viscoelastic fluids are smaller than that of Newtonian fluid and decrease with the increase of DR rate. From Fig. 2 it is seen that drag-reduction is related to not only the magnitude of elastic energy but also its spatial distribution. Fig. 2 shows that the elastic energy of Fluid A is large only in the viscous sublayer; the elastic energy of Fluid B is larger than those of Fluid G and Fluid I in the viscous sublayer but smaller in the buffer layer, and Fluid B has a smaller DR rate than Fluid G and Fluid I; the elastic energy of Fluid F is the same as those of Fluid D and Fluid E in the viscous sublayer but larger in the buffer layer, and it has a larger DR rate. All these show that the occurrence of a large DR rate generally requires a large elastic energy in a wide buffer layer.

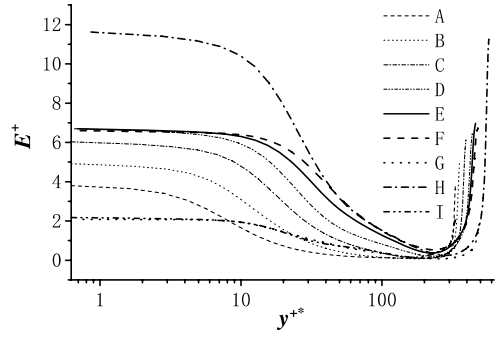

Fig. 2. Mean elastic energy.

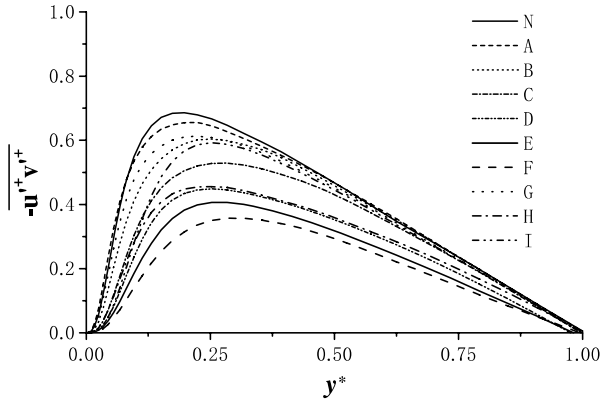

Fig. 3. Reynolds shear stress.

Fig. 3 shows the Reynolds shear stress. Generally, the DR rate is associated with the decrease of Reynolds shear stress but there is not a clear relationship between the two. A maximum DR rate of up to 72% of Fluid F was obtained in the present study, but we did not find a diminish of Reynolds shear stress, which was observed in other experiments (Li et al., 1998). This indicates that the diminish of Reynolds shear stress is not essential for a large DR rate. The Reynolds shear stress of Fluid A is smaller than that of a Newtonian fluid, but no drag-reduction occurs. Fluid C, Fluid G and Fluid I have a similar DR rate but the Reynolds shear stresses differ appreciably. Fluid B has a smaller Reynolds shear stress than Fluid G but a larger DR rate. All the above indicates that a large decrease of Reynolds shear stress does not necessarily mean a large DR rate. Actually, the friction factor is determined by three components: viscous contribution, turbulence contribution, and viscoelastic contribution as follows:

$$C_f = \underbrace{12\beta/Re_b}_{\text{viscous contribution}} + \underbrace{6\int_0^1 \frac{(-\overline{u'^+v'^+})(1-y^*)}{U_b^{+2}}dy^*}_{\text{turbulence contribution}} + \underbrace{6\int_0^1 (1-\beta)\frac{C^+_{xy}}{We_\tau U_b^{+2}}(1-y^*)dy^*}_{\text{viscoelastic contribution}} \quad (4)$$

For a Newtonian fluid, the turbulence contribution is the major component and contributes more than 80% of the friction factor (Yu et al., 2004). Yu et al. (2004) showed that the elastic network structures can decrease the Reynolds shear stress to reduce frictional drag and exert viscoelastic stress to increase frictional drag, and that

drag-reduction occurs because the decrease effect exceeds the increase effect. The quadrant analysis of the Reynolds shear stress provides detailed information on the contributions from various events occurring in the flow. Here we investigate how the Reynolds shear stress changes for different fluids by quadrant analysis. Fluids A–C, F, G and I are compared with Newtonian fluid as shown in Fig. 4. It is seen that for all the viscoelastic fluids the four quadrant events (Q1–Q4) at the bulk flow region are either almost the same as those of the Newtonian fluid or stronger than those of the Newtonian fluid. These stronger events are probably due to the effect of Re_τ^*, i.e. the Re_τ^* of the Newtonian fluid is smaller that those of the viscoelastic fluids. We can expect large values in each quadrant for the Newtonian fluid for larger corresponding Re_τ^*. At the near-wall region, the ejection and sweep events of Fluids B, C, F, G and I are reduced but the outward motion of high-speed fluids (Q1) and the inward motion of low-speed fluids (Q3) are either reduced or enhanced. For Fluid A, the ejection and sweep events do not change as compared to the Newtonian fluid. The decrease of Reynolds shear stress of Fluids B, C, F and I at the near-wall region is due to the reduction of the ejection events (Q2) and sweep events (Q4). For Fluid I, the decrease of sweep events is the largest contribution to the reduction of Reynolds shear stress. However, the decrease of Reynolds shear stress for Fluid G is primarily due to the increase of the outward motion of high-speed fluids (Q1), the inward motion of

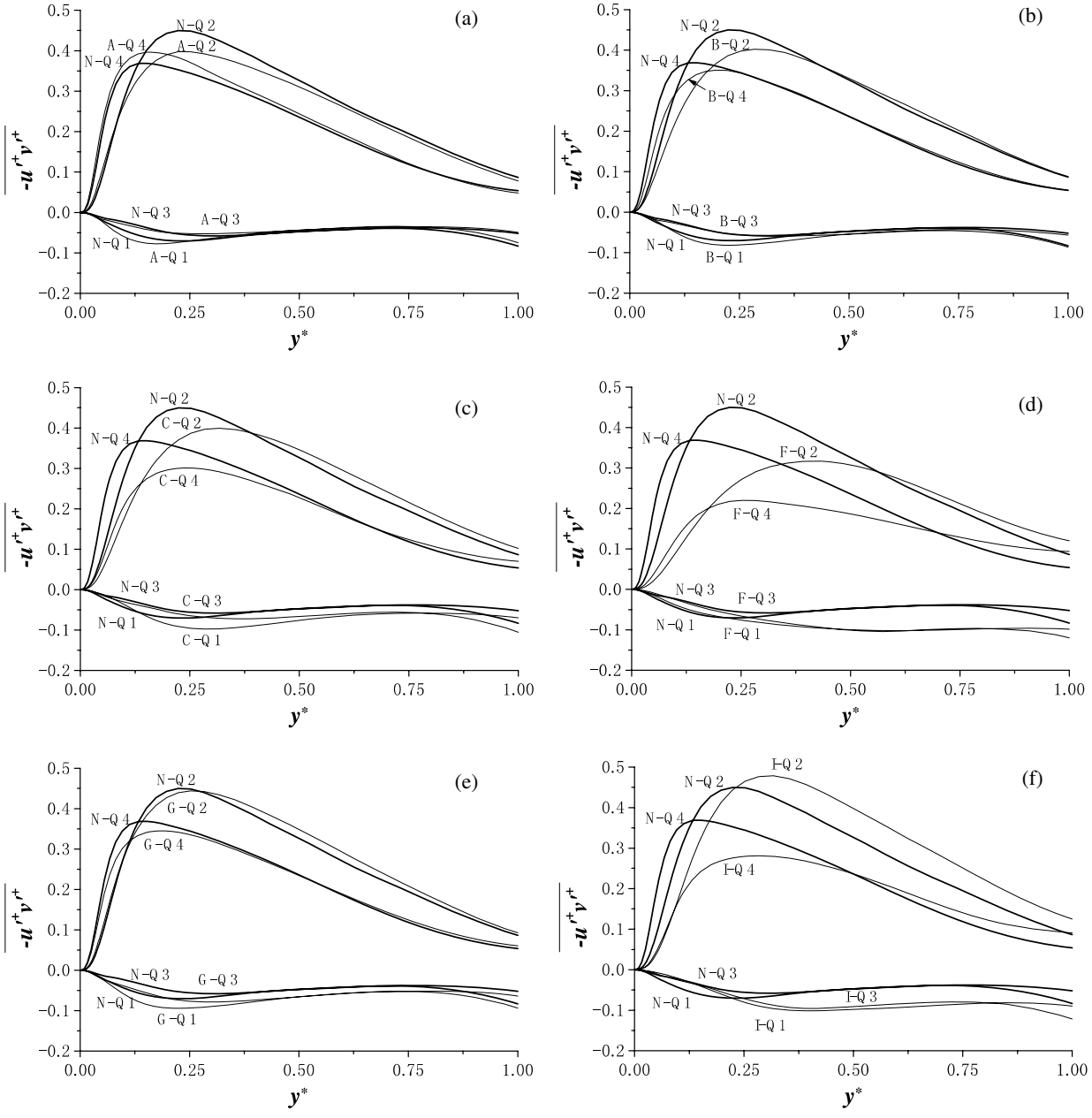

Fig. 4. Reynolds shear stress from each quadrant.

low-speed fluids (Q3), and decrease of sweep events (Q4). In summary, drag-reduction is generally associated with suppression of the ejection and sweep events.

The typical instantaneous streamwise velocity contours, secondary velocity vectors and elastic energy at a cross-section in the y–z plane are shown in Fig. 5. It is seen that the

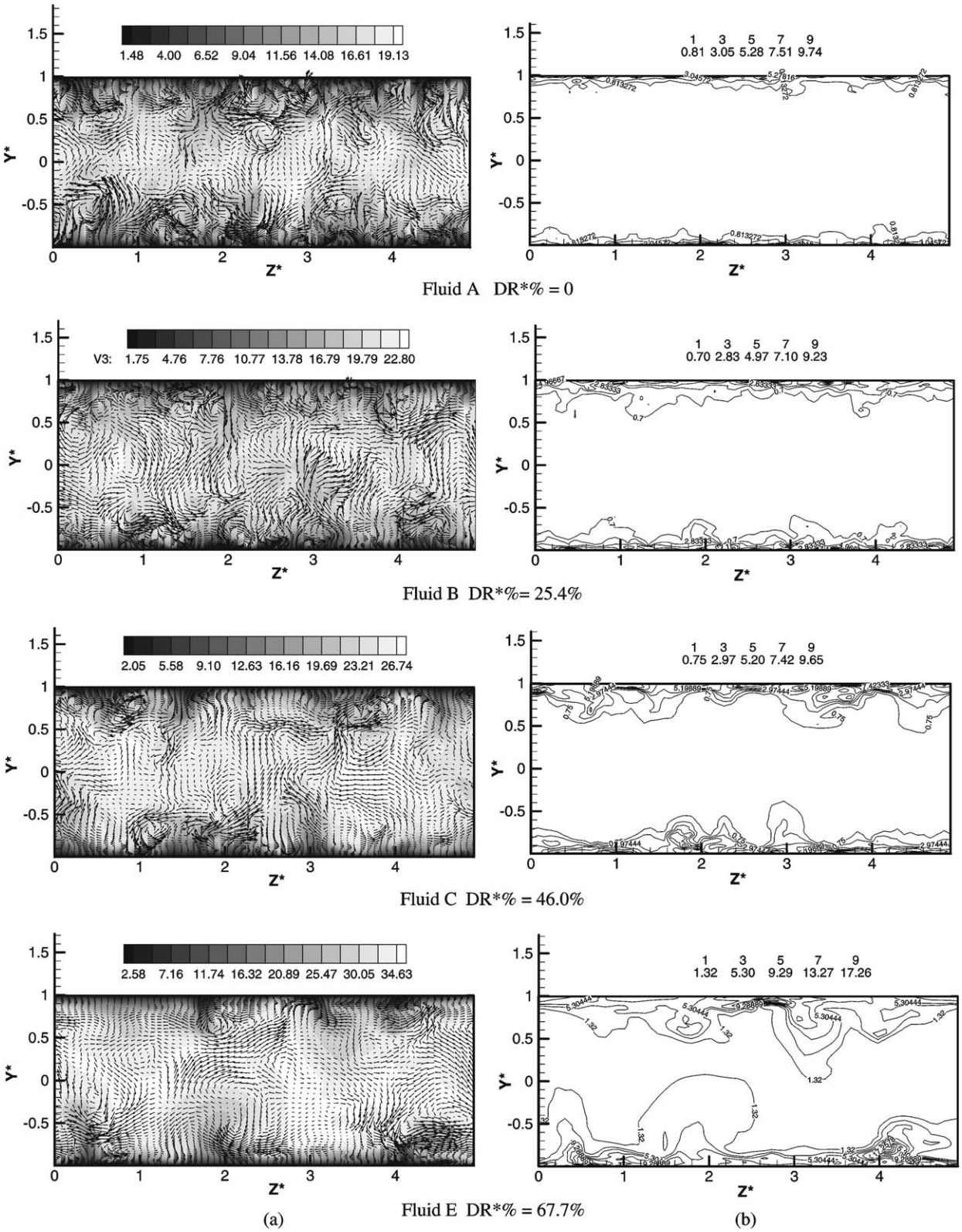

Fig. 5. Instantaneous velocities and elastic energy at a y–z plane. (a) Contour of streamwise velocity and v and w velocity vectors; (b) elastic energy.

spatial size of the circulation becomes larger with the increase of drag-reduction rate. The occurrence of violent outward or wallward motion near the wall is greatly reduced with the increase of DR rates. The region characterized by high elastic energy appears at the same location of outward motion. The isosurfaces of instantaneous streamwise vorticity are shown in Fig. 6, in which the change of vortical structures can be clearly seen. It is seen that the streamwise vorticity becomes much weaker and more elongated with the increase of large drag-reduction rates.

The integrated balance equations of mean kinetic energy, turbulent kinetic energy and elastic energy can be derived as shown below:

$$\underbrace{\int_{-1}^{1}\frac{U^+}{Re_\tau}\mathrm{d}y^*}_{\text{I, Input energy}}=\underbrace{\int_{-1}^{1}-\overline{u'^+v'^+}\frac{\mathrm{d}U^+}{\mathrm{d}y^+}\mathrm{d}y^*}_{\text{II, turbulent production}}+\underbrace{\int_{-1}^{1}\beta\left(\frac{\mathrm{d}U^+}{\mathrm{d}y^+}\right)^2\mathrm{d}y^*}_{\text{III, viscous dissipation}}+\underbrace{\int_{-1}^{1}\frac{1-\beta}{We_\tau}C_{xy}^+\frac{\mathrm{d}U^+}{\mathrm{d}y^+}\mathrm{d}y^*}_{\text{IV, work by viscoelastic stress}} \quad (5)$$

$$\underbrace{\int_{-1}^{1}-\overline{u'^+v'^+}\frac{\mathrm{d}U^+}{\mathrm{d}y^+}\mathrm{d}y^*}_{\text{V, turbulent dissipation}}-\beta\int_{-1}^{1}\overline{\left(\frac{\partial u_i'^+}{\partial x_k^+}\right)\left(\frac{\partial u_i'^+}{\partial x_k^+}\right)}dy^*-\underbrace{\int_{-1}^{1}\frac{1-\beta}{We_\tau}\left(\overline{c_{ik}'^+\frac{\partial u_i'^+}{\partial x_k^+}}\right)\mathrm{d}y^*}_{\text{VI, turbulence-elasticity interaction}}=0 \quad (6)$$

$$\underbrace{\int_{-1}^{1}\frac{1-\beta}{We_\tau}\frac{\mathrm{d}U^+}{\mathrm{d}y^+}C_{xy}^+\mathrm{d}y^*}_{\text{VII, elastic dissipation}}+\int_{-1}^{1}\frac{1-\beta}{We_\tau}\left(\overline{c_{ik}'^+\frac{\partial u_i'^+}{\partial x_k^+}}\right)\mathrm{d}y^*+\int_{-1}^{1}\frac{1-\beta}{2We_\tau^2}[(3-C_{ii}^+)-\alpha(C_{im}^+-\delta_{im})^2]\mathrm{d}y^*=0 \quad (7)$$

Clearly, the energy cascade process for surfactant solutions is quite different from that of the Newtonian fluid. The input energy by the mean pressure gradient is dissipated through path 1 and path 2 as shown in Fig. 7. Path 1 is identical to the Newtonian case. In path 2, the energy is dissipated by the retraction of the network structures.

Fig. 8 shows that the turbulent production and turbulent dissipation are generally smaller than those of the

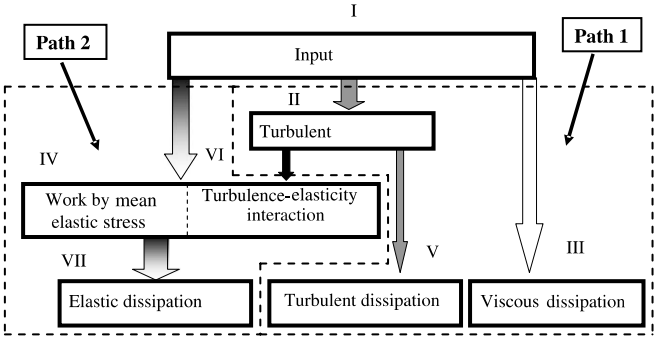

Fig. 7. Energy transport process.

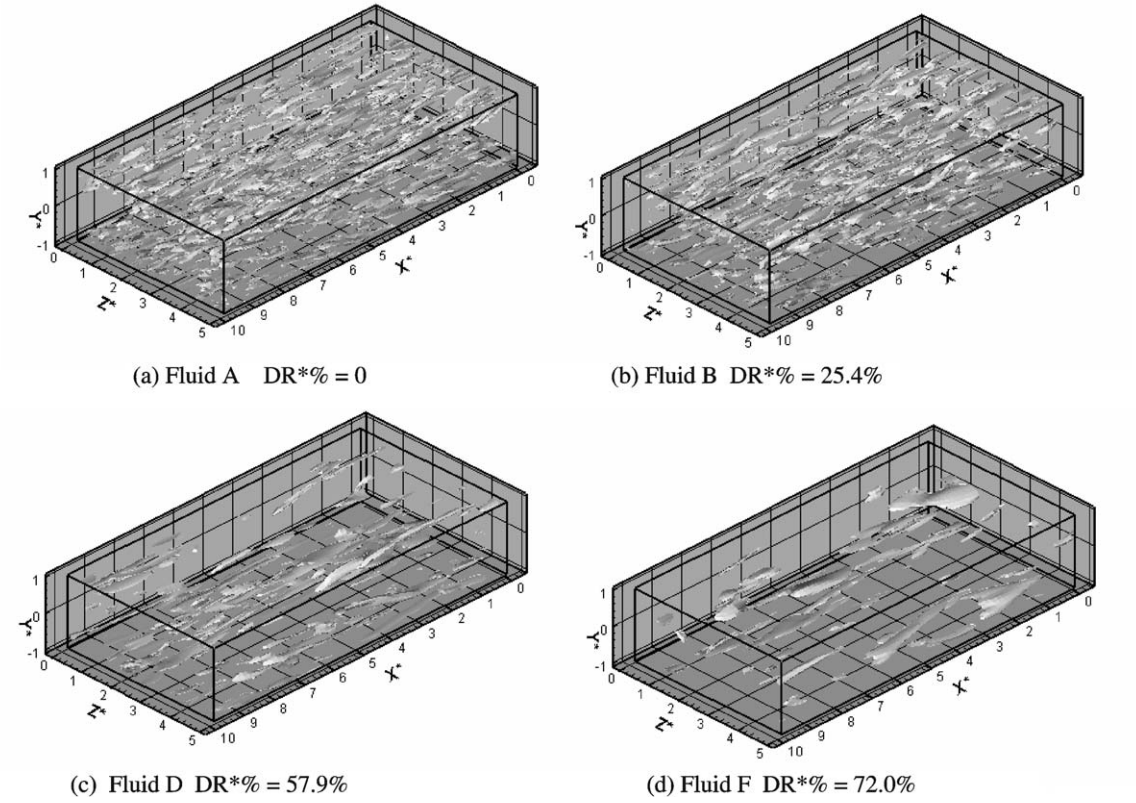

Fig. 6. Isosurfaces of an instantaneous streamwise vorticity $\omega_x = 0.1$.

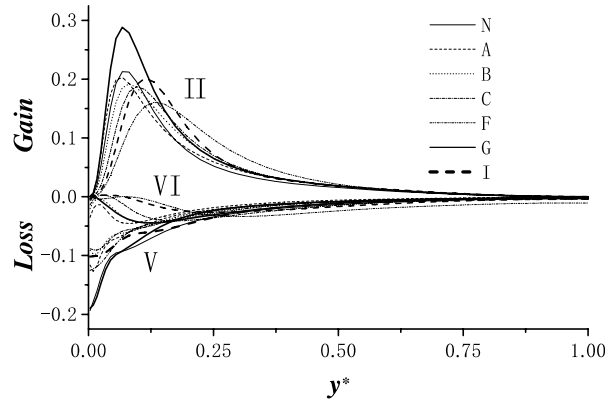

Fig. 8. Turbulent kinetic budget terms.

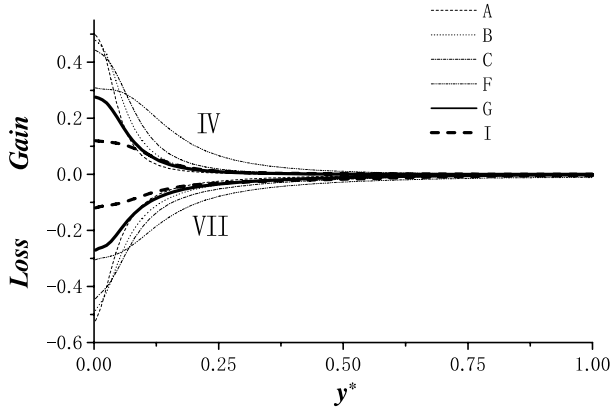

Fig. 9. The elastic energy budget terms IV and VII.

Newtonian fluid except Fluid G. The increase of the turbulent production of Fluid G compared to the Newtonian fluid is because the increase of the velocity gradient is much larger than the decrease of Reynolds shear stress. Note that the increase of the turbulent production corresponds to an increase of input energy due to the increase of mean velocity. A more proper comparison is based on the relative contribution of turbulent production to the total energy. The relative contributions of the turbulent production of the Newtonian fluid and Fluid G are 41% and 34%, respectively. This means that for Fluid G, turbulence has also been effectively suppressed. Turbulence-elasticity interaction acts basically as a sink term, which means that the fluctuating elastic force tends to damp the spatial variation of velocity fluctuations and thereby laminarize the flow. Fig. 9 shows that the large DR rates are associated with large elastic work and elastic dissipation at a wide buffer layer.

The vorticity equation can be derived as follows:

$$\frac{\partial \varpi_i^+}{\partial t^+} + u_j^+ \frac{\partial \varpi_i^+}{\partial x_j^+} = \varpi_j^+ \frac{\partial u_i^+}{\partial x_j^+} + \beta \frac{\partial^2 \varpi_i^+}{\partial x_j^+ \partial x_j^+} + \frac{\varepsilon_{ijk}(1-\beta) Re_\tau}{We_\tau} \frac{\partial}{\partial x_j^+} \left(\frac{\partial c_{kl}^+}{\partial x_l^+} \right) \tag{8}$$

where the first term on the right-hand hand is the vortex stretching term and the last term is due to viscoelasticity. Fig. 10 shows the stretching mode ($\partial u/\partial x > 0$) and squeezing mode ($\partial u/\partial x < 0$) of the streamwise vortex ($\overline{|\varpi_x \partial u/\partial x|}$ is the mean absolute value of $\varpi_x \partial u/\partial x$ over time and x–z plane). It is seen that both the stretching and squeezing modes of the streamwise vortex have been appreciably suppressed at drag-reductions. For Fluid A, the stretching of the streamwise vortex is enhanced as compared to the Newtonian fluid, which is consistent with a smaller vortex size as shown in Table 2.

4. Conclusion

Numerical simulations showed that the drag-reduction rate increases with the increase of We_τ, with the decrease of α and with the decrease of β. Large drag-reduction rate is associated with large elastic energy in the buffer layer. The vortical structures become weaker and more elongated in the streamwise direction and the stretching of the streamwise vortex is greatly reduced for a large drag-reduction rate.

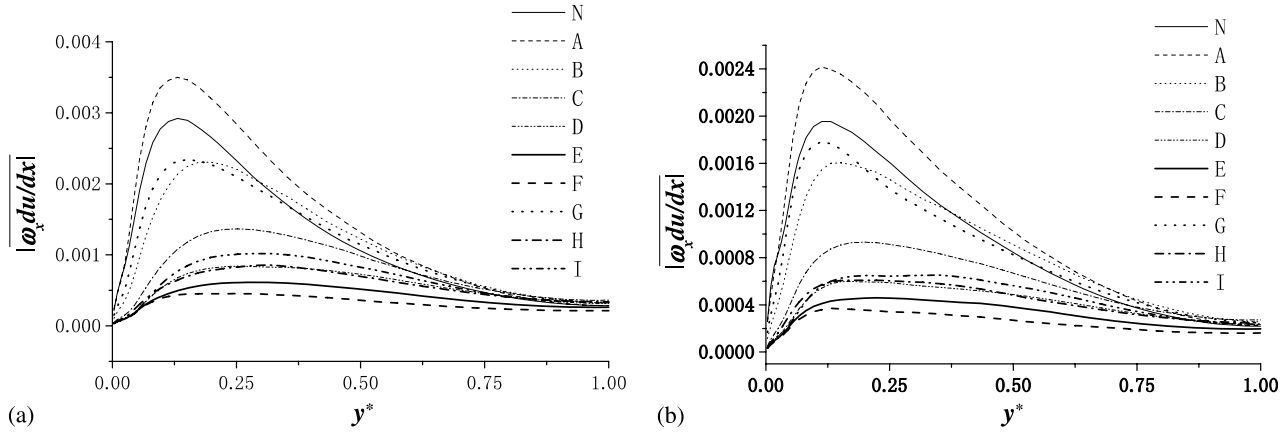

Fig. 10. Intensity of the streamwise vortex stretching: (a) stretching mode, (b) squeezing mode.

Acknowledgement

Yu Bo gratefully acknowledges the support from National Natural Science Foundation of China (No. 50506017).

References

Dean, R.B., 1978. Reynolds number dependence of skin friction and other bulk flow variables in two-dimensional rectangular duct flow. Trans. ASME J. Fluids Eng. 100, 215–223.

Dimitropoulos, C.D., Sureshkumar, R., Beris, A.N., 1998. Direct numerical simulation of viscoelastic turbulent channel flow exhibiting drag reduction: effect of the variation of rheological parameters. J. Non-Newtonian Fluid Mech. 79, 433–468.

Giesekus, H., 1982. A simple constitutive equation for polymer fluids based on the concept of deformation dependent tensorial mobility. J. Non-Newtonian Fluid Mech. 11, 69–109.

Kawaguchi, Y., Wei, J.J., Yu, B., Feng, Z.P., 2003. Rheological characterization of drag-reducing cationic surfactant solution – shear and elongational viscosities of dilute solutions. In: Proceedings of Fluids Engineering Division Summer Meeting, Honolulu, Hawaii.

Li, P.W., Daisaka, H., Kawaguchi, Y., Yabe, A., Hishida, K., Maeda, M., 1998. Experimental investigation of heat transfer enhancement for turbulence drag-reducing flow in a two-dimensional channel. In: Proceedings of Second Fluid Engineering Conference, Manchester, pp. 21–29.

Sureshkumar, R., Beris, A.N., Handler, R.A., 1997. Direct numerical simulation of turbulent channel flow of a polymer solution. Phys. Fluids 9, 743–755.

Yu, B., Kawaguchi, Y., 2004. Direct numerical simulation of viscoelastic drag-reducing flow: a faithful finite difference method. J. Non-Newtonian Fluid Mech. 116, 431–466.

Yu, B., Li, F.C., Kawaguchi, Y., 2004. Numerical and experimental investigation on turbulence structures in a drag-reducing flow with surfactant additives. Int. J. Heat Fluid Flow 25, 961–974.